# Model-Based Segmentation of the Left Atrium in CT and MRI Scans

Birgit Stender[1], Oliver Blanck[2,3], Bo Wang[4], and Alexander Schlaefer[1]

[1] University of Lübeck, Institute for Robotics and Cognitive Systems, Medical Robotics Group, Germany
{stender,schlaefer}@rob.uni-luebeck.de
http://www.rob.uni-luebeck.de/
[2] University Clinic Schleswig-Holstein, Departement for Radiation Oncology, Lübeck, Germany
[3] CyberKnife Center Northern Germany, Güstrow, Germany
[4] Institute of Biomedical Analytical Technology and Instrumentation, Xi'an Jiaotong University, Xi'an, China

**Abstract.** Ablation is a minimal invasive interventional method used in cardiac electrophysiology. It is one option for the treatment of patients suffering from paroxysmal or persistent atrial fibrillation through pulmonary vein isolation. During the intervention endocardial surface potentials from a tracked mapping catheter are recorded with respect to a static patient specific surface geometry. The purpose of the presented work is to compare two different automatic segmentation methods working on both CT and MRI volumes. Segmentation of the left atrium is challenging because the shape variability is high. The use of statistical shape models initialized by means of affine image registration was explored as first method. The second method was non-parametric and based on atlas registration and statistical region growing. Segmentation results were validated and compared using a leave-one-out cross validation on the volumes provided with segmentation results achieved manually by experts. The Dice's coefficient was used as error measure. The method based on statistical region growing performed better than statistical shape models. A Dice's coefficient of 0.87 was achieved on both imaging modalities.

## 1 Introduction

At present the most frequently performed electrophysiological cardiac intervention is ablation therapy for the treatment of atrial fibrillation (AFib). AFib seems to be often caused by abnormal sources of electrical excitation around one or several of the four pulmonary veins leading into the left atrium (LA) [5]. The resulting impairment of an organized atrial contraction is leading to an increased risk of thrombus formation in the left atrium and the left atrial appendage (LAA). In cases of paroxysmal or persistent atrial fibrillation one treatment option is isolation of the ectopic foci achieved by drawing circumferential ablation lines around the pulmonary veins (pulmonary vein isolation, PVI). The catheters approaching the atrial wall to be ablated are displayed in Fig. 1a). During PVIs Electroanatomical Mapping (EAM) systems like Carto$^{TM}$ (Biosense Webster, Diamond Bar, CA, USA) or EnSite NavX$^{TM}$ (St. Jude Medical, St. Paul,

O. Camara et al. (Eds.): STACOM 2013, LNCS 8330, pp. 31–41, 2014.

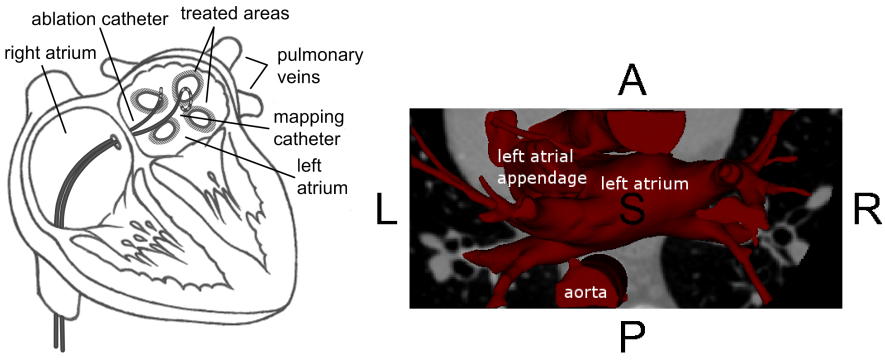


a) b)

**Fig. 1.** a) Target region at the ostia of the pulmonary veins. Ablation and mapping catheter are entering the left atrium penetrating the atrial septum at the fossa ovale. b) Anatomical structures at risk illustrated by segmentation of the blood pool within CT dataset A001.

MN, USA) allow to navigate and record endocardial surface potentials with respect to a static patient specific surface geometry of the blood pool. Because EAM systems allow to navigate the tracked catheters almost in real time the X-ray exposure time caused by fluoroscopic guidance could be reduced for the time period after surface registration.

The accuracy requirements for segmentations of the left endocardial contour are challenging, first, because anatomic structures at risk are located close to the target region and second, because the ablation lines need to be drawn with high precision. As illustrated in Fig. 1b) anatomical structures at risk are the left atrial appendage (LAA) and the aorta. The esophagus not visible in Fig. 1b) is potentially also located close to the left atrial wall.

Improvement in left atrial segmentation could be achieved by addressing the following two sub-problems:

1. Fully automatic segmentation of the atrial endocardial contour in contrast-enhanced CT could reduce the preparation time and increase the reproducibility of this first step within the clinical workflow.
2. The substitution of CT with MRI as preoperative imaging modality would be desirable to further reduce the X-ray exposure of the patients. Currently the quality of the segmentation results is not as good as the one achieved in CT volumes. A further improvement of segmentation algorithms working in MRI and a detailed investigation of the results in direct comparison with CT data would allow an evidence-based decision making between the two imaging modalities.

Among the most recently published papers on left atrial segmentation the majority was focusing on MRI. Several authors pointed out that the contour of the left atrium is highly variable [4,12,8]. A relatively simple approach presented was based on segmentation of the blood pool and subsequent determination of cutting planes at narrowings [7]. Due to the inhomogeneous and patient-specific distribution of imaging gray values within the blood pool user-interaction was required. A segmentation algorithm based

on registration of an atlas and labelmap fusion was already presented at the STACOM conference in 2010 by Depa et al. [4]. A very recently presented approach is based on splitting the complex structure of the contour into simpler substructures. The parts are then segmented using multi-model statistical shape knowledge [12,8].

We will present two different approaches. The first one is based on statistical shape models (SSM), the second one uses region growing. Both approaches utilize atlas information for initialization and work fully automatically.

## 2 Material and Methods

### 2.1 Material

The two segmentation approaches were tested with the 30 CT and 30 MRI volumetric scans of the Left Atrial Segmentation Challenge 2013 database. The imaging data was recorded using cardiac gating and contrast enhancement. Ground truth is provided through segmentations performed by clinical experts. The training datasets A for CT and MRI include 10 volumetric scans and ground truth labelmaps for each modality. The remaining 20 volumetric scans each given without ground truth will be referred in the following as CT dataset B and MRI dataset B. The mean spatial resolution is 0.45 mm for the CT and 1.25 mm for the MRI volumetric scans. Further information on the patients' anamnesis and the imaging protocols used was not provided.

### 2.2 Modality Specific Atlases of the Left Atrium

The quality of segmentation results achieved with SSM in general strongly depends on accurate initialization [6]. Usually the initial pose (position and orientation) of the mean shape is selected interactively which can be time-consuming and is potentially leading to user-dependent segmentation results. To overcome these known drawbacks we automatically determined the pose for the initial contour by means of atlas registration. This technique was used as well to initialize the statistical region growing approach. For this second approach seed points and assumptions on the range of gray values were automatically generated.

Two modality specific atlases were determined from CT dataset A and MRI dataset A. The volumes were cropped around the LA annotations within the corresponding labelmap. One of the LA volumes was selected as reference. It will be annotated as *ref* in the following. Pairwise affine registration was performed to map all LA volumes $i \neq ref$ in dataset A onto LA volume *ref*.

An affine registration algorithm is optimizing 12 parameters describing position, orientation, scaling and shearing by minimizing the mutual information similarity measure between two volumes. The result is a 4 x 4 transformation matrix ${}^{ref}H_i$ which describes the transformation of voxels from image volume $i$ to image volume *ref*. We used the Fast Affine Registration and ResampleVolume2 modules released as part of 3D Slicer 3.6.3 for affine registration throughout the whole work [9]. Slicer modules were called via shell scripts. Histogram equalization and averaging of the transformed image volumes resulted in a mean volume used as template. These steps were performed in Matlab.

In Fig. 2 the result for CT is shown. The left (right) column images are all displayed with respect to the same coronal (transverse) cutting plane. The reference volume is displayed in Fig. 2 a) and b), the mean volume used as template in c) and d) and the probability density distribution in e) and f).

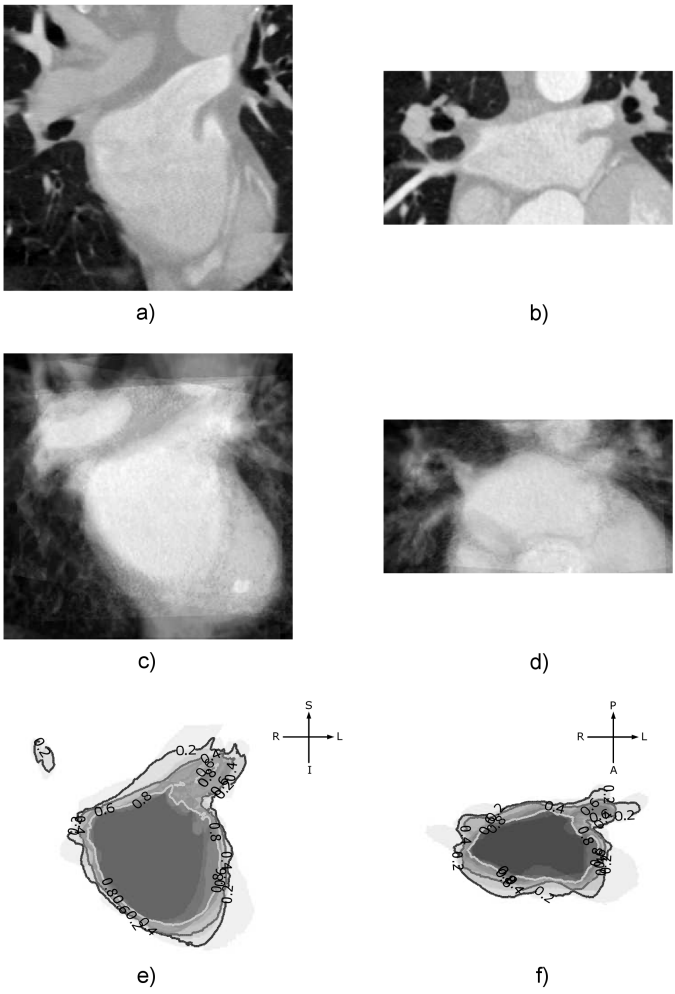


**Fig. 2.** a) and b): CT volume A003 used as reference dataset *ref*. c) and d): Atlas template volume created from the CT training dataset A. e) and f): Propability density distribution of the volume to belong to the blood pool of the left atrium.

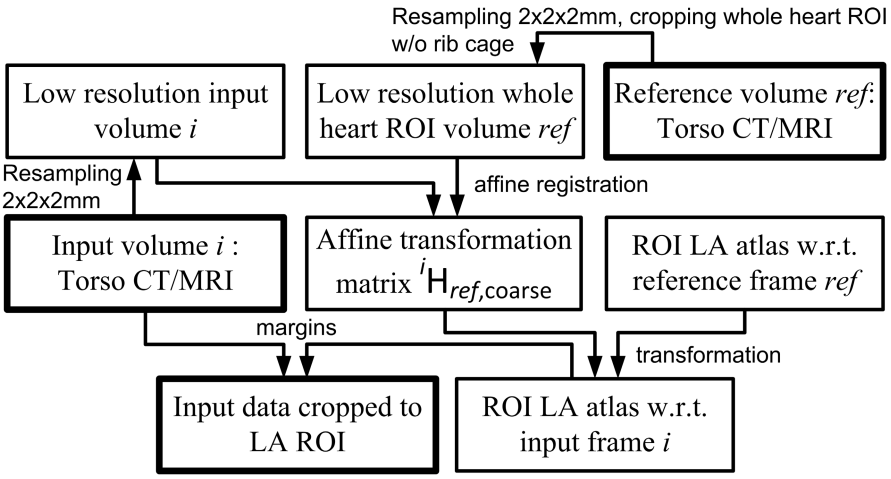


**Fig. 3.** Workflow for left atrial ROI detection in a CT or MRI input volume to be segmented

### 2.3 Identifying the Left Atrial Region of Interest

The workflow for detection of the LA ROI is displayed Fig. 3. In a first step the whole torso reference volume *ref* and the input torso volume $i$ to be segmented were downsampled isotropically to a resolution of 2 mm. Within the downsampled reference volume an ROI including a large region of the heart is cropped without parts of the rib cage. The rib cage is excluded because the dimensions of the skeletal bones and the dimensions of the heart are not correlated in deseased patients.

Affine registration of the heart region to the input dataset resulted in the transformation matrix $^{i}H_{ref,\mathrm{coarse}}$. This transformation matrix describes the position, orientation, scaling and shearing of the reference image volume *ref* with respect to the input image volume *i*. Because the modality specific atlas was determined with respect to the reference volume the margins of the atlas volume were also defined with respect to this image volume. The rectangular LA atlas ROI was transformed with the affine transformation matrix $^{i}H_{ref,\mathrm{coarse}}$ to determine the LA ROI with respect to the volume $i$. Within the input volume in its original resolution the LA ROI was then cropped as starting point for the initialization of the two segmentation algorithms.

### 2.4 Statistical Shape Models

SSM are a set of methods which has already been successfully applied to various medical image segmentation tasks. While active shape models (ASM) include prior knowledge of the mean shape and its variations, active appearance models (AAM) are additionally augmented with statistical knowledge of imaging features associated with the contour [3,2,6].

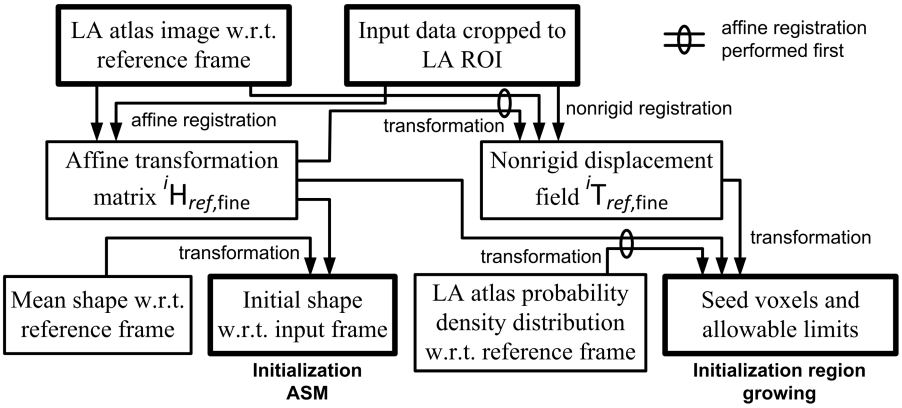


**Fig. 4.** Initialization workflow for both segmentation algorithms. By means of atlas registration the initial contour for the segmentation approach using a statistical shape model was determined as well as the initial volume and margins for segmenation based on statistical region growing.

**Initialization Based on Image Registration.** The segmentation algorithm started with an affine registration of the atlas image onto the input volume as shown in Fig. 4. The mean contour was afterwards mapped using the same affine transformation matrix. This initial contour guess is constrained by the permitted variations of the SSM.

**The Point Distribution Model.** For representation of the mean shape and shape variability a point distribution model (PDM) was used. Such a PDM is built up in the following steps: The groundtruth annotations within all $N$ image volumes are described by a certain number $k$ of landmark points on the contour. The $3k$ landmark point coordinates for each contour $i$ are listed in the column vector $\mathbf{x}_i = (x_1, \ldots, x_k, y_1, \ldots, y_k, z_1, \ldots, z_k)$. Assuming known point-to-point correspondences among the landmark points the mean shape is then determined by simply averaging over the $3k$ point coordinates:

$$\bar{\mathbf{x}} = \frac{1}{N} \sum_{i=1}^{N} \mathbf{x}_i \tag{1}$$

By means of an eigendecomposition on the sample covariance matrix

$$\mathbf{S} = \frac{1}{N-1} \sum_{i=1}^{N} (\mathbf{x}_i - \bar{\mathbf{x}}) (\mathbf{x}_i - \bar{\mathbf{x}})^T , \tag{2}$$

the eigenvectors $\phi_m$ and the corresponding eigenvalues $\lambda_m$ are determined. Permissable shape variations are modeled as linear combination of the eigenvectors with the largest eigenvalues.

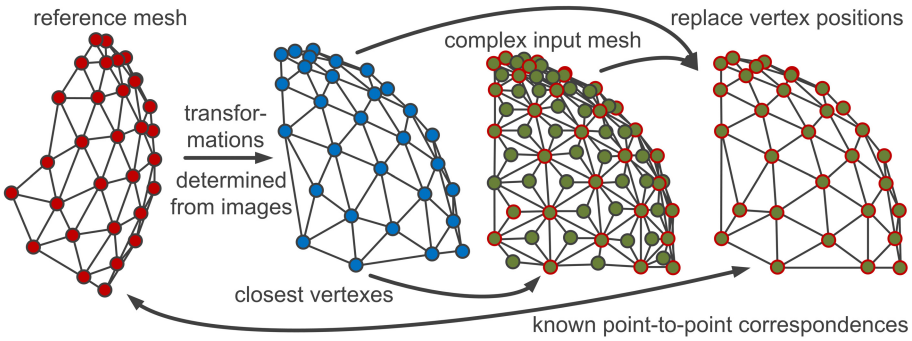


**Fig. 5.** Surface transformation based on image registration

**Point-to-Point Correspondences.** Setting up the PDM presupposes known point-to-point correspondences between the different surface meshes. The shapes further need to be aligned which is usually done with Procrustes or generalized Procrustes analysis (GPA) based on the vertex points. We used instead the affine transformation matrices determined during atlas construction as illustrated in Fig. 5. From the ground truth labelmap of the reference dataset (A003 for CT, A002 for MRI) a simplified surface mesh was created (2000 vertexes for CT, 500 vertexes for MRI). Within Fig. 5 this mesh is represented by the one on the left hand side with red vertexes. From the other groundtruth labelmaps complexer surface meshes (10,000 vertexes for CT, 2500 vertexes for MRI) were computed. One of these meshes is the one with green vertexes in Fig. 5. The same affine registration algorithm and settings as used for building the atlases were applied to register the reference volume onto each of the nine other volumes included in dataset A. Subsequently non-rigid transformation fields were computed with the same demons registration algorithm and settings as used for registering the atlases onto a previously unseen volume. The resulting affine transformation matrix and nonrigid transformation field were used for warping the vertexes of the simplified reference mesh. The operation is displayed in Fig. 5 as transformation from the red mesh to the blue one. For reasons of clarity the blue mesh is not displayed superimposed with the green mesh. For each vertex included in the blue mesh the closest vertex within the green mesh was identified (green vertexes with red borders). The vertex coordinates of each blue vertex were than replaced with the ones of the closest vertex. The connectivity remained unchanged.

**Shape Adaptation.** After initialization the contour is propagated in each adaptation step along the surface normals of the vertexes. The step size is determined based on gradient features. After adaptation the shape is tested for successful representation within the shape space confidence intervals.

### 2.5 Stastical Region Growing

Statistical region growing is a segmentation algorithm based on a search algorithm. For all voxels within an intermediate segmentation result the mean intensity value is

determined. The voxels within a certain neighborhood of the intermediate segmentation result are listed in a queue. A voxel from the queue is inserted into the intermediate segmentation result if its intensity value difference from the mean is within certain limits. Its voxel neighborhood is then added to the queue. The algorithm terminates if the queue is empty. Instead of using a single voxel as seed point we started with all voxels having a high probability to be part of the LA.

The probability distribution was determined by atlas registration using affine and susequent non-rigid registration as illustrated in Fig. 4. The Fast Symmetric Forces variant of Thirion's demons algorithm was used as non-rigid registration algorithm [10,11]. The basic algorithm uses the following modified version of the optical flow equation for the pixel shift $\mathbf{u}$

$$\mathbf{u} = \frac{(m-f)\nabla f}{|\nabla f|^2 + (m-f)^2}, \tag{3}$$

where $m$ and $f$ denote the intensity values of the fixed and moving image. The term $(m-f)^2$ has a stabilizing effect. For the affine and subsequent non-rigid registration we called the Fast Affine Registration and BRAINSDemonWarp module released as part of 3D Slicer 3.6.3 via shell scripts [9].

Instead of updating the limits within the statistical region growing algorithm at each iteration the mean and standard deviation of the image gray values were determined from the set of seed voxels. A 26-voxel neighborhood was used. The threshold around the mean image gray value was set to $\pm 1.5\sigma$ for CT and $\pm 3\sigma$ for MRI. We implemented the algorithm in C++ and called it as Matlab mex-file. Afterwards the filter module Voting Binary Hole Filling Filter within 3D Slicer 3.6.3 was applied [9]. The parameters selected were: majority threshold 1, maximum radius 6 for CT and 3 for MRI.

## 3 Results

### 3.1 Cross Validation

For quantitative comparison of the segmentation results we used the Dice's coefficient $\mathbf{dc}\,(\mathbf{SR}, \mathbf{GT})$ as similarity measure between the set of segmented voxels $\mathbf{SR}$ and the set of ground truth voxels $\mathbf{GT}$. To explore the capability of initialization based on image registration we first validated results from affine and non-rigid registration without any further segmentation steps. Each ground truth labelmap was therefore transformed to the grid of the remaining images within training dataset A. The transformations applied resulted from registration of the underlying images. The Dice's coefficients from registration are listed in line (a) and (b) of Tab. 1. The mean for affine registration was 0.64 for CT ad 0.74 for MRI. These values were increased by 8.8% for MRI and by 22.1% for CT trough additionally applied non-rigid registration. The standard deviation was also raised from 0.10 (CT) and 0.06 (MRI) to 0.11 for both imaging modalities.

Using statistical region growing with atlas based initialization in a leave-on-out cross validation scheme the mean Dice's coefficient could further be increased to 0.87 for both imaging modalities in comparison to affine and subsequent non-rigid registration only. For further details please refer to Tab. 1 line (c). The standard deviation of the dice coefficient was reduced to a third. The segmentation results achieved with SSM

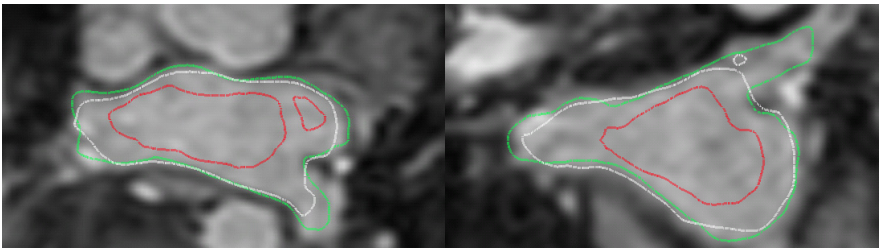

a) b)

**Fig. 6.** Segmentation result achieved with statistical region growing on MRI volume A001 (dice coefficient 0.88) displayed for an axial cutting plane (a) and a coronal cutting plane (b). Red contour: Seed voxels as given by the registered probability density distribution of the atlas with value equal to 1. White contour: Segmentation result. Green contour: Ground truth provided.

(Tab. 1 line (d)) were again similar for both imaging modalities and a did not outperform the results from statistical region growing (0.83 mean Dice's coefficient for MRI and CT).

### 3.2 Computational Complexity

The computing times required are listed in Tab. 2. All computations were performed on a Windows XP Professional x64 operating system. The CPU was an Intel Xeon CPU 5160 running at 3.00 GHz. 15.9 GB of RAM was installed. For statistical region growing initialization by means of atlas registration (Step: Determination of seed voxels) accounted for 82.2% (CT) and 96.8% (MRI) of the computational effort.

**Table 1.** Dice's coefficients for the left atrium in CT and MRI using only registration (affine (a), affine and subsequent non-rigid (b)) in comparison to results achieved with the two segmentation approaches ((c) and (d))

| | | mean | std | min | max |
|---|---|---|---|---|---|
| **(a) Affine registration** | CT | 0.6383 | 0.0965 | 0.1846 | 0.8266 |
| | MRI | 0.7414 | 0.0639 | 0.5598 | 0.8447 |
| **(b) Non-rigid registration** | CT | 0.7794 | 0.1053 | 0.4619 | 0.9373 |
| | MRI | 0.8070 | 0.1062 | 0.0412 | 0.9121 |
| **(c) Statistical region growing** | CT | 0.8674 | 0.0289 | 0.8123 | 0.9038 |
| | MRI | 0.8706 | 0.0333 | 0.8084 | 0.9001 |
| **(d) Statistical shape model** | CT | 0.8271 | 0.0528 | 0.7307 | 0.8808 |
| | MRI | 0.8303 | 0.0559 | 0.7003 | 0.9024 |

**Table 2.** Computing time for the different steps of the segmentation algorithms given in sec.

| | | CT | MRI |
|---|---|---|---|
| **Statistical region growing** | Determination of seed voxels | 383.96 | 15.06 |
| | Region growing | 0.98 | 0.03 |
| | Hole Filling Filter | 82.00 | 0.47 |
| | **Sum** | **466.94** | **15.56** |
| **Statistical shape models** | Affine transformation | 16.39 | 6.57 |
| | Model adaptation | 215.52 | 13.55 |
| | Affine Backtransformation | 16.39 | 6.57 |
| | **Sum** | **248.30** | **26.69** |

This was mainly caused by non-rigid image registration of the atlas volume using the original imaging resolution (up to 0.3 mm for CT, up to 0.75 mm for MRI). For SSM the largest share of the computational costs was caused by the iterative shape model adaption step (86.8% for CT, 50.8% for MRI). In total the computational time for SSM was 46.8% lower for CT and 71.5% higher for MRI in comparison to statistical region growing.

## 4 Discussion and Conclusion

We demonstrated two methods for automatic segmentation of the endocardial contour of the left atrium. The approaches are applicable to CT and MRI. The first method is based on image registration and statistical region growing. A seed voxel volume and a mask for the image volume containing the left atrium were generated based on atlas registration. This approach is non-parametric because it is not based on a certain parameterization of the contour.

The second approach is using SSM. The shape and its variations are explicitly represented by means of a point distribution model. The property of being non-parametric is an advantage in case of high variability of the anatomical shape. As already pointed out at the STACOM 2010 by Depa et al. this is especially the case for the anatomy of the pulmonary veins leading into the left atrium [4]. Because two veins can built a common trunk not even the number must necessarily be constant. In addition comparison of ground truth contours achieved within MRI and CT images revealed that in CT the contours typically propagated further into the pulmonary veins but to different extents within the volumes included in dataset A.

The number of volumes given with corresponding ground truth is quite limited and therefore most likely not a sufficient representation of the whole space of shape variations. This is reflected by the fact that statistical region growing outperformed the approach based on SSM with respect the Dice's coefficient. However, there are also limitations of statistical region growing, as indicated by leaking within the left ventricle or the aortic root in some image volumes. Furthermore a higher computing time was required for initialization in CT images.

Within the clinical workflow the computational complexity of the algorithms is not the most important feature. Typically CT or MRI images are recorded on the day before. In addition preparation of the patients in the catheter lab takes several minutes.

The computing time of the non-rigid registration included might be reduced by down-sampling the CT volumes in this step without substantially affecting the quality of the segmentation results afterwards. The results also indicate, that it may be interesting to study a hybrid approach including statistical region growing around the pulmonary veins after convergence of the shape adaptation of the SSM. This would allow to segment a larger range of anatomical variations among pulmonary vein anatomy while still preventing leaking into the aortic root and left ventricle by the restrictions modeled within the shape space.

**Acknowledgements.** This work was partially supported by BMBF grant 01EZ1140A.

## References

1. Aliot, E., Ruskin, J.N.: Controversies in ablation of atrial fibrillation. European Heart Journal Supplements 10(supp. H), H32–H54 (2008)
2. Cootes, T.F., Edwards, G.J., Taylor, C.J.: Active appearance models. Pattern Anal. Mach. Intell. 23(6), 681–685 (2001)
3. Cootes, T.F., Taylor, C.J., Cooper, D.H., Graham, J.: Active shape models - their training and application. Comput. Vis. Image Und. 61(1), 38–59 (1995)
4. Depa, M., Sabuncu, M.R., Holmvang, G., Nezafat, R., Schmidt, E.J., Golland, P.: Robust Atlas-Based Segmentation of Highly Variable Anatomy: Left Atrium Segmentation. In: Camara, O., Pop, M., Rhode, K., Sermesant, M., Smith, N., Young, A. (eds.) STACOM 2010. LNCS, vol. 6364, pp. 85–94. Springer, Heidelberg (2010)
5. Hassaguerre, M., Jas, P., Shah, D.C., Takahashi, A., et al.: Spontaneous initiation of atrial fibrillation by ectopic beats originating in the pulmonary veins. N. Engl. J. Med. 339(10), 659–666 (1998)
6. Heimann, T., Meinzer, H.-P.: Statistical shape models for 3D medical image segmentation: A review. Medical Image Analysis 13(4), 543–563 (2009)
7. John, M., Rahn, N.: Automatic left atrium segmentation by cutting the blood pool at narrowings. In: Duncan, J.S., Gerig, G. (eds.) MICCAI 2005. LNCS, vol. 3750, pp. 798–805. Springer, Heidelberg (2005)
8. Kutra, D., Saalbach, A., Lehmann, H., Groth, A., Dries, S.P.M., Krueger, M.W., Dössel, O., Weese, J.: Automatic Multi-model-Based Segmentation of the Left Atrium in Cardiac MRI Scans. In: Ayache, N., Delingette, H., Golland, P., Mori, K. (eds.) MICCAI 2012, Part II. LNCS, vol. 7511, pp. 1–8. Springer, Heidelberg (2012)
9. Pieper, S., Lorensen, B., Schroeder, W., Kikinis, R.: The NA-MIC Kit: ITK, VTK, Pipelines, Grids and 3D Slicer as an Open Platform for the Medical Image Computing Community. In: Proceedings of the 3rd IEEE International Symposium on Biomedical Imaging: From Nano to Macro, vol. 1, pp. 698–701 (2006)
10. Prima, S., Thirion, J.-P., Subsol, G., Roberts, N.: Automatic analysis of normal brain dissymmetry of males and females in MR images. In: Wells, W.M., Colchester, A.C.F., Delp, S.L. (eds.) MICCAI 1998. LNCS, vol. 1496, pp. 770–779. Springer, Heidelberg (1998)
11. Vercauteren, T., Pennec, X., Perchant, A., Ayache, N.: Diffeomorphic Demons: Efficient Non-parametric Image Registration. Neuroimage, 45(1 suppl.), S61–S72 (2009)
12. Zheng, Y., Wang, T., John, M., Zhou, S.K., Boese, J., Comaniciu, D.: Multi-part left atrium modeling and segmentation in C-arm CT volumes for atrial fibrillation ablation. In: Fichtinger, G., Martel, A., Peters, T. (eds.) MICCAI 2011, Part III. LNCS, vol. 6893, pp. 487–495. Springer, Heidelberg (2011)